ELSEVIER

Journal of Nuclear Materials 266–269 (1999) 709–713

journal of nuclear materials

Erosion, redeposition and boronization lifetime in RFX

L. Tramontin [a,*], V. Antoni [a,b], M. Bagatin [a,b], D. Boscarino [c], E. Cattaruzza [c], V. Rigato [d], S. Zandolin [c]

[a] *Consorzio RFX – Corso Stati Uniti, 4-35127 Padova, Italy*
[b] *Unità I.N.F.M., Dipartimento di Ingegneria Elettrica, Università di Padova, via Gradenigo, 6/A-35131 Padova, Italy*
[c] *Unità I.N.F.M., Dipartimento di Fisica, Università di Padova, via Marzolo, 8-35131, Padova, Italy*
[d] *Laboratori Nazionali di Legnaro (INFN), via Romea, 4-35020 Legnaro, PD, Italy*

Abstract

In this paper the boronization lifetime in the reversed field pinch experiment RFX is discussed. It is found that the redeposition of carbon-rich layers, which grow during plasma exposure, cover the boron containing layers preventing the getter effect through formation of stable boron oxides. Enhanced localized erosion on graphite tiles, which constitute the first wall of the experiment, due to magnetic disturbances or field errors is identified as the source of carbon which codeposits together with hydrogen over the boronized layers. Samples covered with different boron containing layers have been exposed to the plasma, analyzed by surface techniques and compared. The redeposition process is confirmed to be the main cause determining the boronization lifetime.

Keywords: Reversed field pinch; RFX; Boronization; Co-deposition

1. Introduction

RFX, a Reversed Field Pinch (RFP) experiment ($r = 2$ m, $a = 0.457$ m) [1], has a first wall made of 2016 graphite tiles which cover the metallic vessel and no limiter is present. The graphite tiles are subjected to strong energy fluxes and heavy particle bombardment by hydrogen and impurities. Erosion phenomena are observed to dominate in narrow regions of strong plasma–surface interaction, whereas larger regions in proximity of the eroded areas are subjected to redeposition. In principle a well centred discharge would induce a uniform plasma–wall interaction with an average energy flux of $\sim$0.5 MW/m^2 for a plasma current of 500 kA. However in all of the discharges a stationary magnetic perturbation due to phase-locked MHD modes [2] gives rise to an enhanced plasma–wall interaction in a region $\leqslant 1/40$ of the total surface. The interaction is mainly localized at the edges of the graphite tiles which are invested by the energy and particle fluxes parallel to the magnetic field [3]. It has been observed that magnetic field errors at the diagnostic ports induce a similar process. There are many evidences from CCD cameras and spectroscopic measurements [3] that this concentrated interaction leads to impurity influxes two orders of magnitude larger than the average one.

Since 1994 boronization processes, similar to those applied to tokamaks [4,5], have been performed in RFX using $B(CH_3)_3$ and B_2H_6 in order to improve the plasma performances mainly in term of impurity content (oxygen) and in term of operations at higher density [6]. The deposition of the boron containing coating needs repetitive applications since the beneficial effects are limited in time. In this paper the boronization lifetime is discussed in connection with the redeposition of carbon-rich layers which are shown to grow during plasma exposure covering the boron containing layers and preventing the formation of stable boron oxides.

To investigate this effect, surface collector probes have been used as a tool. They were analyzed by ion beam techniques and X-ray photoelectron spectroscopy. The structure of the boron containing layers deposited

* Corresponding author. Tel.: +39-049 829 5975; fax: +39-049 870 0718; e-mail: tramontin@igi.pd.cnr.it

0022-3115/99/$ – see front matter
PII: S0022-3115(98)00837-X

by boronization, as well as the effects of particle fluxes impinging on boronized surfaces have been examined. The redeposition mechanisms have been interpreted in terms of codeposition phenomena. The results have then been extended to the regions of the first wall where plasma–surface interaction similar to that of the collector probe is expected.

2. Experimental

Samples have been exposed to a plasma with toroidal plasma current of 500–650 kA and an average electron density of $2 - 6 \times 10^{19}$ m^{-3}. In similar discharges the plasma edge parameters have been evaluated by Langmuir and calorimetric probes [7]: the density shows a steep gradient $\nabla n \sim 10^{21}$ m^{-4}, whereas the edge electron temperature is of the order of 10 eV with a gradient of $\nabla T \sim 700$ eV m^{-1}. The magnetic field at the edge is ~ 0.2 T and mainly poloidal since the toroidal component is typically 10 times lower. The hydrogen and carbon Larmor radii are 2 and 8 mm respectively assuming $T_i \approx T_e$. The radial particle flux, mainly driven by electrostatic fluctuations [8], is of the order of 10^{22} m^{-2} s^{-1}, corresponding to a particle confinement time of $\sim$1 ms. The corresponding diffusion coefficient at the edge has been estimated to be of the order of 10–20 m^2/s for hydrogen and impurities [9]. It is found that superthermal electrons flowing along the magnetic field lines [10] give rise to parallel energy fluxes of the order of 100 MW/m^2 with a consequent thermal load at the edges of the carbon tiles that intercept the field lines and face these electrons [7].

Silicon samples were inserted, by means of a driving system [11], in the equatorial plane of RFX and were placed at $r/a \geqslant 1.01$ in the scrape off layer (SOL) inside the diagnostic access protected from the superthermal electrons. The collector probes were mounted on a graphite cylindrical sample holder (Fig. 1) equipped with six lateral slits which allowed to expose the samples with their surface at different angles, α, with respect to the local magnetic field, **B**. A collector probe could also be mounted on the top of the cylinder so that the magnetic field lines were parallel to the probe surface. After exposure to the plasma the silicon samples, precleaned in diluted hydrofluoric acid and in ultrasonic bath, were transferred in air to the analysis facilities.

Ion beam analyses, carried out with a 2.2 MV and a 7 MV Van de Graaff accelerators, were used to determine the areal densities and depth profiles of the elements in the collector probes. The carbon and oxygen contents were simultaneously measured by means of ^{12}C(d,p)^{13}C and ^{16}O(d,p)^{17}O non-resonant nuclear reactions using a 620 keV deuteron beam. A 660 keV proton beam was used to measure the ^{11}B content by means of the ^{11}B(p,α)^{8}Be non-resonant nuclear reaction. The hydrogen content was estimated by elastic recoil detection analysis (ERDA) with a 2.2 MeV He$^+$ beam. Resonant nuclear reactions, ^{1}H(^{15}N,$\alpha\gamma$)^{12}C, with detection of γ-rays were also used for hydrogen depth profiling. The layer composition and the chemical bonds as a function of depth were determined by XPS (X-ray Photoelectron Spectroscopy) using Al K_α radiation (1486.6 eV). The spectrometer was calibrated using the binding energy, E_B, of the Ag3d$_{5/2}$ line at 386.2 eV with respect to the Fermi level as standard. The atomic composition was evaluated using standard sensitivity factors. The analysis as a function of depth was carried out by sputtering with an Ar beam.

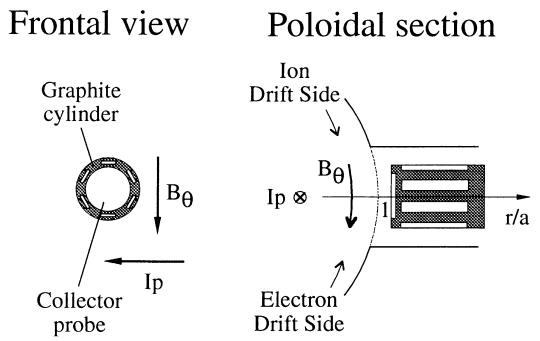

Fig. 1. Schematic view of the graphite sample holder. The coordinate r/a is the radial position normalized to the minor radius. At the inner convolution of the graphite first wall $r/a = 1$.

In the following results will be presented which refer to three experimental campaigns:

- Two silicon samples were exposed to boronization in B(CH3)$_3$. They were mounted on the top of the graphite cylinder at the radial position corresponding to the inner graphite wall and kept at the same potential. One of them was extracted and analyzed by XPS, ERDA and NRA. It was then replaced by a pure silicon sample which was exposed, together with the remaining boronized sample, to about 40 plasma discharges with $I_p = 500$ kA, $n_e = 4 \times 10^{19}$ m^{-3} and 50–100 ms duration, not immediately after boronization but about 50 discharges later. Both these samples were analyzed by XPS, ERDA and NRA.
- A silicon sample, located on the top of the sample holder, was exposed to B_2H_6 boronization. After analysis with XPS, ERDA and NRA, it was exposed to about 30 plasma discharges ($I_p = 640$ kA, $n_e = 3 \times 10^{19}$ m^{-3} and $\tau = 100$–150 ms) long after boronization. Again it was analyzed by XPS, ERDA and NRA.
- Silicon samples were exposed for 3.2 s to plasma discharges with $I_p < 500$ kA, $n_e = (2 - 4) \times 10^{19}$ m^{-3} and 50–90 ms duration. They were located on the six lateral slits of the sample holder and were analyzed by ERDA and NRA.

3. Results and discussion

3.1. Plasma exposure of boronized samples

The results of a boronization process in a mixture of He and $B(CH_3)_3$ and the composition of the resulting boronized layer have already been reported in [6]. The layer, ~60 nm thick, consisted mainly of carbon, boron and hydrogen with B/C = 0.44 ± 0.03 and H/(B + C) = 0.42 ± 0.04. Oxygen was only found at the interface between the layer and the silicon substrate.

Boronizations in a mixture of He and B_2H_6 at a wall temperature of 250°C were also performed. The deposited layer consisted of boron and hydrogen with a H/B ratio of less than 0.2. A hydrogenated carbon film was observed between the boron containing layer and the silicon substrate, which was formed before boronization during the He and H glow discharge cleaning procedures. In the following sample A and sample B will indicate the silicon samples exposed to boronization with $B(CH_3)_3$ and to boronization with B_2H_6, respectively. Samples A and B were subsequently exposed to plasma discharges with their surface parallel to the local magnetic field lines, at $r/a \geqslant 1.01$.

Fig. 2 shows the atomic concentration depth profile of sample A after exposure to plasma discharges. It was measured by combining ion sputtering and XPS. The depth scale was obtained by direct measurements with a mechanical profilometer. The profile may be divided into three regions that correspond to the silicon substrate (I), the film deposited during boronization (II) and the redeposited layer grown during plasma exposure (III). It is important to note that region II in Fig. 2 exactly corresponds to the boronized layer measured by the same technique on sample A before plasma exposure.

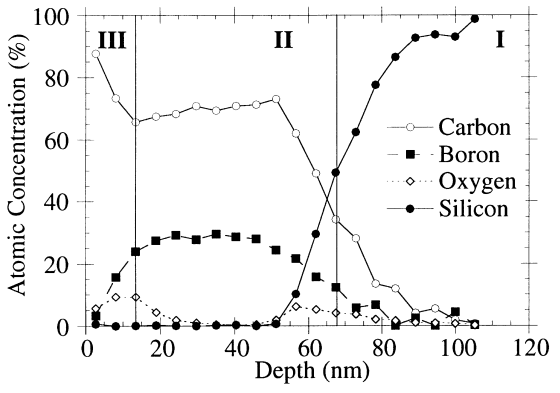

Fig. 2. XPS atomic concentration depth profile of the sample A exposed to boronization in $B(CH_3)_3$ and subsequently to 40 plasma discharges. The I region is the silicon substrate, II indicates the layer deposited during boronization and III is the layer grown during plasma exposure.

Two main features emerge from the XPS analysis:

(a) Oxygen is observed to accumulate at the interface between the boronized layer (II) and the redeposited layer due to plasma exposure (III). The binding energy value of the main component in B1s peak, relative to the region of maximum oxygen concentration, is 191.0 ± 0.1 eV and indicates the formation of non-stoichiometric boron oxides [12]. The B1s peak sets to the binding energy value of 189.1 ± 0.1 eV in the bulk boronized layer where oxygen is not present. It is known that the oxygen build-up depends not only on the gettering effect but also on the processes of sticking and absorption from air [13]. The strong reduction of oxygen impurity in the plasma [6] suggests that, as reported in reference [13], the gettering effect plays a main role also in RFX.

(b) A carbon-rich layer, about 10–15 nm thick, is deposited during plasma discharges in 3.8 s. The C1s binding energy value, relative to the redeposited layer, is 284.6 ± 0.1 eV and is typically assigned to hydrogenated carbon compounds [14]. At larger depths (>10 nm) the binding energy shifts towards lower values, 284.0 eV, associated to the formation of carbidic bonds. The redeposition of a hydrogenated carbon layer is substantiated by an increase in hydrogen and carbon areal densities measured by ERDA and NRA on sample A after plasma exposure. This carbon-rich layer, that grows as a function of the exposure time, prevents oxygen to reach boron and to form non-volatile boron oxides.

Hydrogen and impurity amounts were also measured on the silicon sample exposed to the same plasma discharges and in the same position as sample A. Hydrogen and carbon areal densities are comparable and equal $\sim 4 \times 10^{20}$ m^{-2}, whereas the boron amount is ~30 times lower. The particle influxes during sample exposure were obtained by monitoring emission spectra of H_α and CII. The hydrogen influx varied between $0.3-1.5 \times 10^{22}$ m^{-2} s^{-1}, whereas the carbon influx was two order of magnitude lower with an average value of $\sim 0.5 \times 10^{20}$ m^{-2} s^{-1} [6]. This latter value, that equals the carbon outflux in stationary conditions, cannot account by itself for the carbon amount deposited on the sample in 3.8 s. An enhanced outflux due to localized interaction is likely to account for the observed carbon deposition rate.

The B/C areal densities on the redeposited layer in sample A after 50 discharges is ~0.03, much lower than B/C ~0.44 in the boronized layer. Depletion of B/C on redeposited layers in the SOL has been reported in TEXTOR [15] and interpreted as a reduction of the boron content at the surface of the limiter. In RFX, where no single limiters are present, this behaviour can be interpreted as due to the combination of localized erosion and prompt redeposition. Indeed enhanced

plasma–wall interaction, as discussed in the introduction, causes the complete erosion of the boronized layers, as confirmed by inspection of the graphite tiles [16]. The C atoms, thermally released from the graphite substrate, are expected to promptly redeposit within 0.1 m from the source [7] because of the large Larmor radius, diffusion processes and field errors. As discussed in the introduction, locked modes are the main cause of this enhanced plasma–wall interaction. Since these modes lock to the wall in a toroidal location which changes randomly shot by shot, then after 50–100 discharges the coating of the whole first wall is likely affected.

A similar B/C depletion is observed on sample B (Fig. 3) which was exposed to the plasma ~300 discharges after B_2H_6 boronization. The figure shows the XPS atomic concentration depth profiles where the depth scale was obtained by conversion of the sputtering time scale using an erosion speed of 1.5 nm/min obtained by a reference sample. As in sample A, oxygen accumulates at the interface between the boronized layer (II) and the redeposited layer (III). In the region of maximum oxygen concentration the XPS analysis indicates the formation of non-stoichiometric boron oxides, as derived from the B1s binding energy (191.0 ± 0.1 eV). A carbon-rich layer, about 10 nm thick, builds up despite the fact that the first wall was completely covered by a carbon-free coating. This film, which buries the boronized layer after ~30 discharges, is characterized by graphitic bonds derived by the C1s binding energy values (284.5 ± 0.1 eV). This observation reinforces the hypothesis that carbon originates from localized spots in regions affected by the locked mode perturbation, where the boronized layer is completely eroded. NRA and ERDA measurements indicate that carbon and hydrogen collection rates are similar to those measured on sample A after exposure.

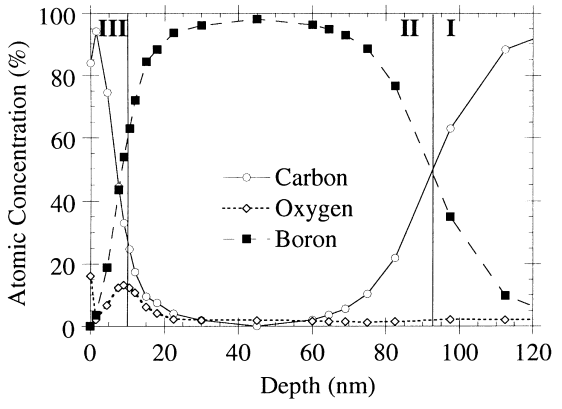

Fig. 3. XPS atomic concentration depth profile of the sample B exposed to boronization in B_2H_6 and subsequently to 30 plasma discharges. The I region is the hydrogenated carbon layer formed during H and He glow discharge cleaning procedures performed before boronization, II indicates the layer deposited during boronization and III is the layer grown during plasma exposure.

3.2. Redeposition

Redeposition was investigated in more detail by analyzing the surface of silicon collector probes mounted in the six lateral locations of the sample holder and exposed to the SOL for a total exposure time of 3.2 s. Measurements of hydrogen and carbon redeposition were performed on each collector probe at different radial positions, using ERDA and $^{12}C(d,p)^{13}C$ reaction analysis techniques respectively. The redeposition reaches its maximum on the sample closer to the edge of the tile protecting the diagnostic access and facing the electron drift side. Fig. 4 shows the atomic ratio H/C as a function of the carbon areal density. For carbon deposition greater than $\sim 5 \times 10^{20}$ m^{-2}, measured on the samples facing the local source, the hydrogen over carbon ratio tends to a saturation value of about 0.55. In codeposition experiments with energetic deuterium ions [17], a saturation value H/C ~0.4 is found. For areal density below 5×10^{20} m^{-2} the H/C ratio increases up to 1.5. It is worth noting that similar values are found in polymerlike films [18,19]. On the other hand, the contribution of H initially implanted in the Si substrate cannot be ruled out because of the limited depth resolution of the analysis techniques. However, according to reference [20], with the estimated ion implantation energy ($\leqslant 50$ eV), this contribution results <1/3 of the H content at the lower C concentration and negligible at the higher C concentration.

In Fig. 5 the hydrogen depth profile measured by NRA using a 6.5 MeV $^{15}N^{2+}$ beam is shown. The γ counts are plotted as a function of depth which is de-

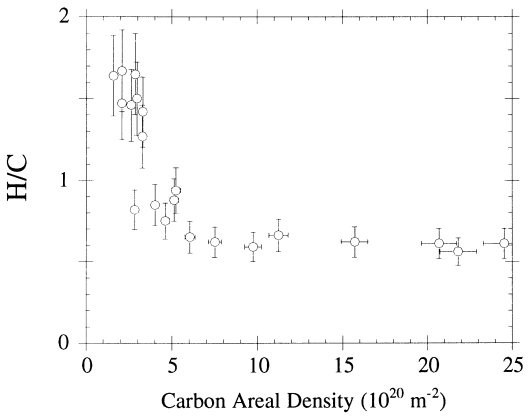

Fig. 4. Hydrogen over carbon atomic ratio versus carbon areal density.

rived with a stopping power of 127×10^{-15} eV cm^2 [21] in a substrate made of hydrogen and carbon assuming a constant H/C = 0.5. The depth profile indicates that hydrogen atoms extend into the substrate at depths of some tens of nm, larger than the ion implantation range (1–2 nm) for ions with an impact energy of some tens eV.

An estimate of the total carbon flux, which may be compared to atomic and molecular influxes, is obtained by the carbon concentration measured radially on the collector probe closer to the source. The average parallel carbon flux $\Gamma_{//} \sim 2.5 \times 10^{21}$ m^{-2} s^{-1} in the SOL, obtained by normalizing the net carbon concentration to the total exposure time, is characterized by an e-folding length $\lambda_C \approx 8$ mm. A radial carbon outflux of $\sim 8 \times 10^{20}$ m^{-2} s^{-1} results from a simple particle balance, with a SOL connection length $L \approx 25$ mm defined by the geometry and without source terms. This value is ten times larger than the average carbon influx [22] and confirms that it is due to the enhanced localized interaction. The resulting carbon diffusion coefficient is ~ 15 m^2/s comparable to the hydrogen and impurity diffusion coefficients measured in the edge plasma at 300–400 kA [9].

4. Conclusions

The boronization lifetime in RFX is shown to be mainly limited by carbon redeposition processes. Redeposition of thick ($\sim$10 nm) carbon-rich layers in tens of discharges, has been measured on collector probes exposed to the plasma after boronizations with $B(CH_3)_3$ or B_2H_6. The redeposited layers consist mainly of hydrogen and carbon that codeposit on the substrate. The carbon source has been identified in localized enhanced plasma–wall interaction at the edge of the graphite tiles invested by magnetic field lines. Since redeposition of thermally released impurities has been proved to occur promptly, the boronized film becomes buried in a region close to the source within a few discharges. Magnetic disturbances due to wall locked modes are believed to be the main cause for these effects. Taking into account the spatial extension and random localization shot to shot of these disturbances, this leads to a limit of the boronization lifetime in RFX of 50–100 discharges, in agreement with present estimates for 500–600 kA plasma current discharges.

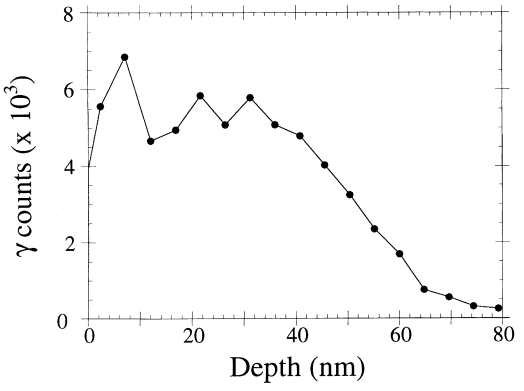

Fig. 5. Hydrogen depth profile measured by $^1H(^{15}N,\gamma\alpha)^{12}C$ resonant nuclear reaction. The γ counts are plotted as a function of depth.

References

[1] G. Rostagni, Fusion Eng. Des. 25 (1995) 315.
[2] V. Antoni et al., 22nd EPS Conf. Plasma Phys. and Controlled Fusion, Bournemouth, vol. IV, 1995, p. 181.
[3] M. Valisa et al., J. Nucl. Mater. 241–243 (1997) 988.
[4] J. Winter et al., J. Nucl. Mater. 162–164 (1989) 713.
[5] J. Winter et al., J. Nucl. Mater. 176&177 (1990) 486.
[6] P. Sonato et al., J. Nucl. Mater. 227 (1996) 259.
[7] V. Antoni et al., J. Nucl. Mater. 220–222 (1995) 650.
[8] V. Antoni et al., Phys. Rev. Lett. 80 (1998) 4185.
[9] M. Bagatin et al., these Proceedings.
[10] Y. Yagi et al, Plasma Phys. and Contr. Fusion 39 (1997) 1915.
[11] M. Bagatin et al., Fusion Eng. Des. 25 (1995) 425.
[12] R. Zeheringer et al., J. Nucl. Mater. 176&177 (1990) 370.
[13] P. Wienhold et al., J. Nucl. Mater. 196–198 (1992) 647.
[14] H. Künzli et al., J. Nucl. Mater. 196–198 (1992) 622.
[15] P. Wienhold et al., J. Nucl. Mater. 176&177 (1990) 150.
[16] P. Sonato et al., J. Nucl. Mater. 241–243 (1997) 982.
[17] M. Mayer et al., J. Nucl. Mater. 230 (1996) 67.
[18] W. Möller, Appl. Phys. A 56 (1993) 527.
[19] M. Langhoff, B.M.U. Scherzer, J. Nucl. Mater. 245 (1997) 60.
[20] G. Staudenmaier et al., J. Nucl. Mater. 84 (1979) 149.
[21] J.F. Ziegler, J.P. Biersack, The Stopping and Range of Ions in Solids, Pergamon, New York, 1995.
[22] L. Carraro et al., J. Nucl. Mater. 220–222 (1995) 646.